Preparation of bis-Schiff base immobilized mesoporous SBA-15 nanosensor for the fluorogenic sensing and adsorption of Cu^{2+}

Yuanyuan Zhang[a]*, Tao Zhu[a], Huiyan Wang[b], Liangliang Zheng[a], Ming Chen[a], Wenyong Wang[c]

a School of Environmental and Chemical Engineering, Jiangsu Ocean University, Lianyungang, 222005, P. R. China

b Jiangsu Key Laboratory of Function Control Technology for Advanced Materials, Jiangsu Ocean University, Lianyungang, 222005, P. R. China

c Jiangsu Xinhai Senior High School, Lianyungang, 222005, P. R. China

*Corresponding author:

✉*E-mail: zhangyy@jou.edu.cn*

DFT Theoretical calculation

The theoretical calculations were performed using Gaussian 09 program. The grafted bis-Schiff base was chosen as the computation model. Full geometrical optimization of the complex was carried out using the B3LYP functional of the density functional theory (DFT) calculation method without any symmetry constraints, C, H, O, N atoms were described by 6-3 G(d, p) basis set, SDD relativistic pseudo-potentials was applied for the simulation of Cu^{2+} ions [1]. Natural bond orbital (NBO) analysis was simulated by the level of theory with B3LYP/6–311++G (d, p) [2].

The binding energy was determined according to the difference between the total energy of complex, and the energy of isolated bis-Schiff base ligand and Cu^{2+}.

$$\Delta E = E(\text{complex}) - [E(\text{adsorbent}) + E(Cu^{2+})] \quad (1)$$

where E is the total energy calculated using the single-point energy calculations on the basis of the geometry optimization (B3LYP/6-311+G (d, p) level, SDD for metal ions).

Table S1 Textural and structural properties of SBA-15, MS-DEA, MS-CSA and MS-NSP.

Samples	BET surface area (m^2/g)	Pore volume (mL/g)	Pore diameter (nm)
SBA-15	687	1.02	5.1
MS-DEA	300	0.57	4.5
MS-CSA	168	0.34	4.4
MS-NSP	122	0.27	4.2

Table S2 Comparison of the detection limit of MS-NSP toward Cu^{2+} with other reported fluorescence nanosensors.

Nanosensor	Ions	Detection Limit	References
Naphthalimide modified SBA-15	Cu^{2+}	1.0×10^{-9} M	[3]
BODIPY incorporated magnetic nanomaterial	Cu^{2+}	1.0×10^{-6} M	[4]
5-Methoxy-2-thiazole grafted SBA-15	Cu^{2+}	1.0×10^{-6} M	[5]
Anthracene modified mesoporous silica	Cu^{2+}	2.0×10^{-8} M	[6]
Schiff base-grafted mesoporous silica	Cu^{2+}	0.8×10^{-6} M	[7]
Naphthalimide-functionalized magnetic nanoparticles	Cu^{2+}	2.8×10^{-7} M	[8]

Table S3 Kinetic equation constants

Ions	Pseudo-first-order		Pseudo-second-order		
	k_1	R^2	k_2	Q_e	R^2
Cu^{2+}	0.02752	0.8707	0.0076	23.81	0.991

Table S4 Langmuir and Freundlich isotherm model parameters.

Metal ion	Langmuir model			Freundlish model		
Cu^{2+}	K_L	Q_m	R^2	1/n	K_F	R^2
	0.012	58.45	0.9939	0.5414	2.437	0.9788

Table S5 Binding energy and bond length for bis-Schiff base complex.

complex	Binding energy （kcal/mol）	Bond length (Å)	
		N–Cu	O–Cu
ligand with Cu^{2+}	–407.8	1.94	2.01

Table S6 NBO partial charges, electron configurations and dipole moments for bis-Schiff base.

complex	NBO partial charges		Cu^{2+} Electron Configuration[a]	Dipole moment (D)[b]
	Ligand	Cu^{2+}		
ligand with Cu^{2+}	0.97	1.03	$4S^{0.35}3d^{9.34}4p^{0.284}d^{0.01}$	3.61

[a]Ground-state electron configuration of free Cu^{2+} is $3d^9$.

[b]Dipole moments of free Schiff base ligand is 3.37 D.

.

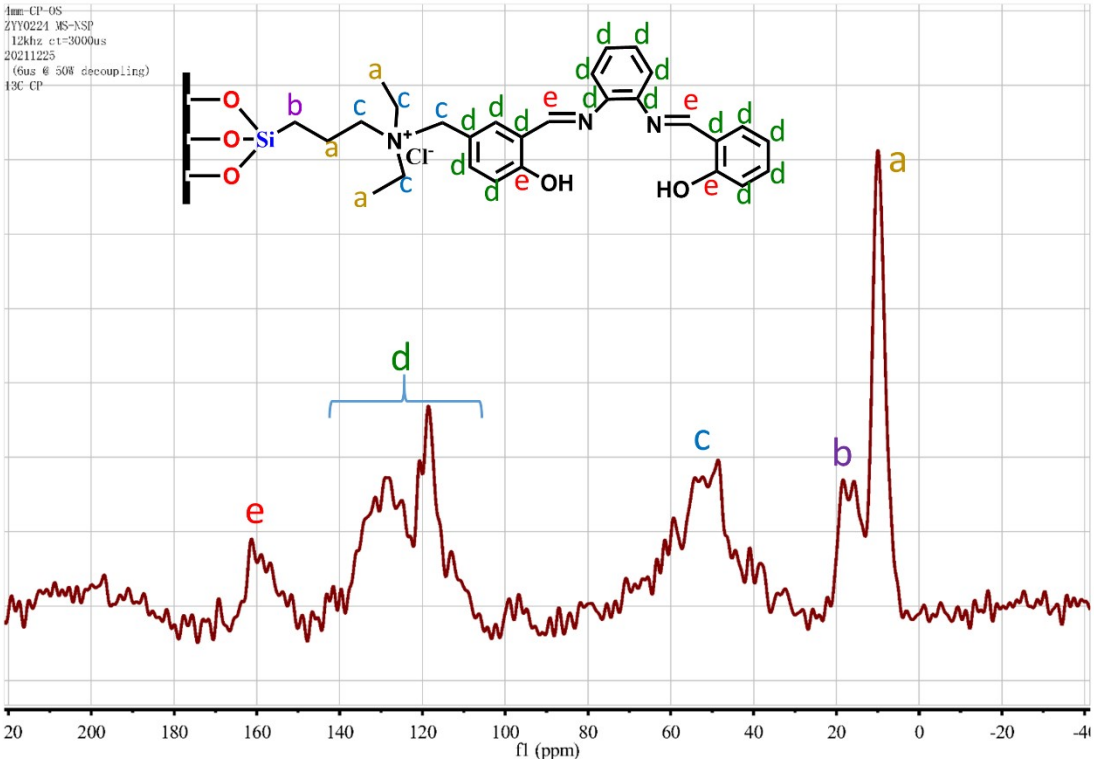

Fig. S1 ^{13}C CP-MAS NMR spectrum of MS-NSP.

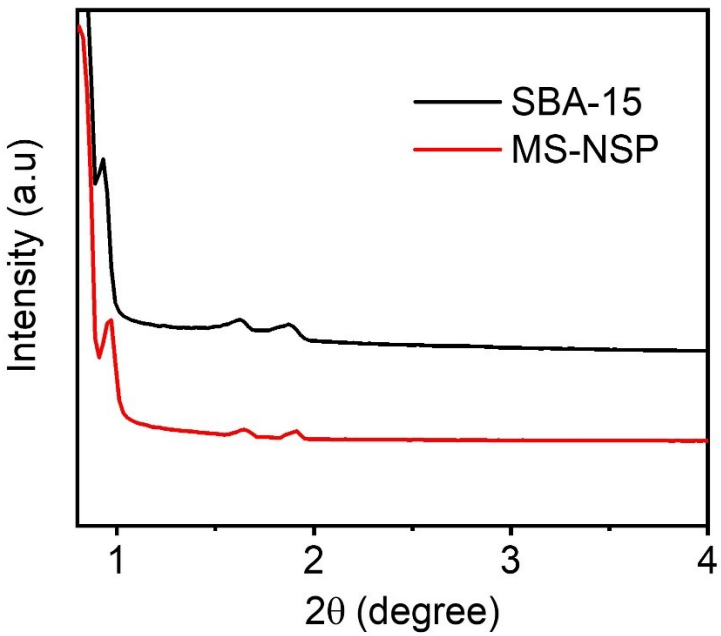

Fig. S2 Low-angle XRD patterns of pristine SBA-15 and MS-NSP

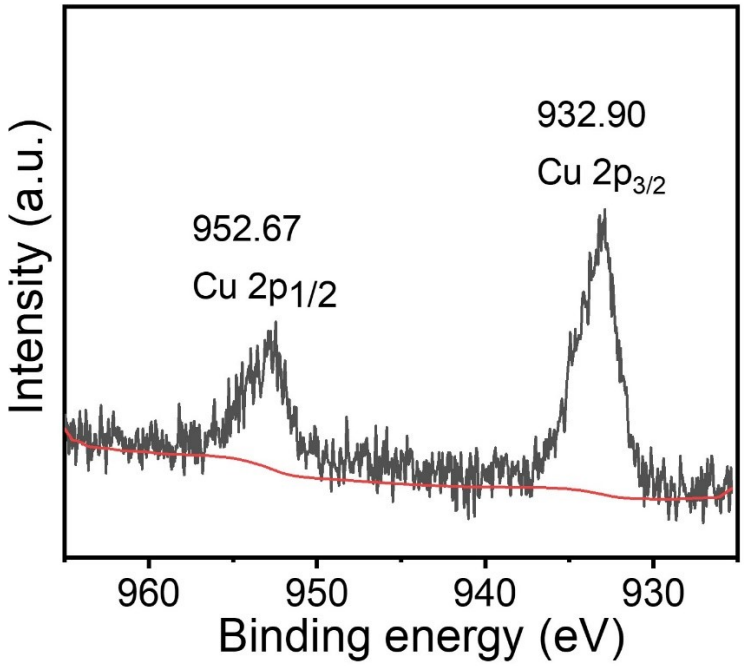

Fig. S3 Cu2p XPS spectrum of Saloph(Cu)-SBA.

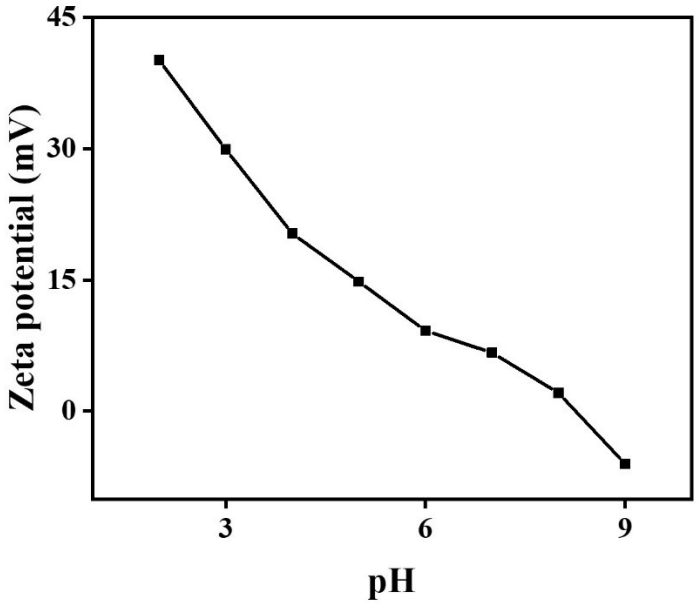

Fig. S4 Zeta potential of MS-NSP as a functional of pH values.

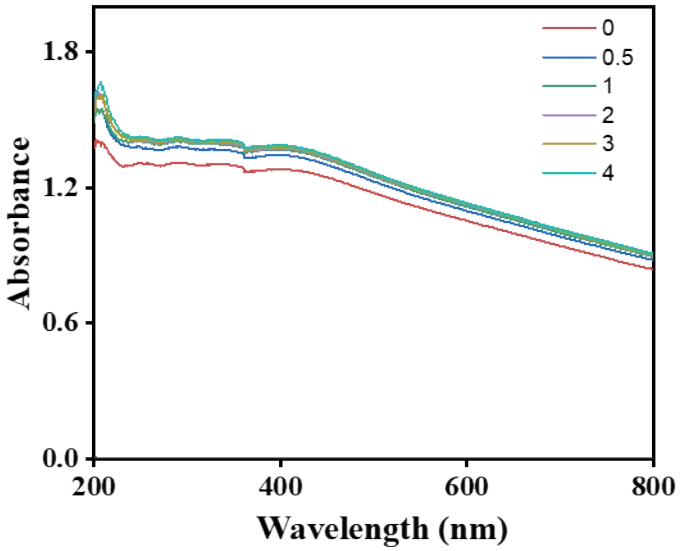

Fig. S5. The change of UV–vis absorption spectra of MS-NSP (0.25 mg/mL) in water upon addition of Cu^{2+} with different concentrations (0–4 mg/L) at 25 °C.

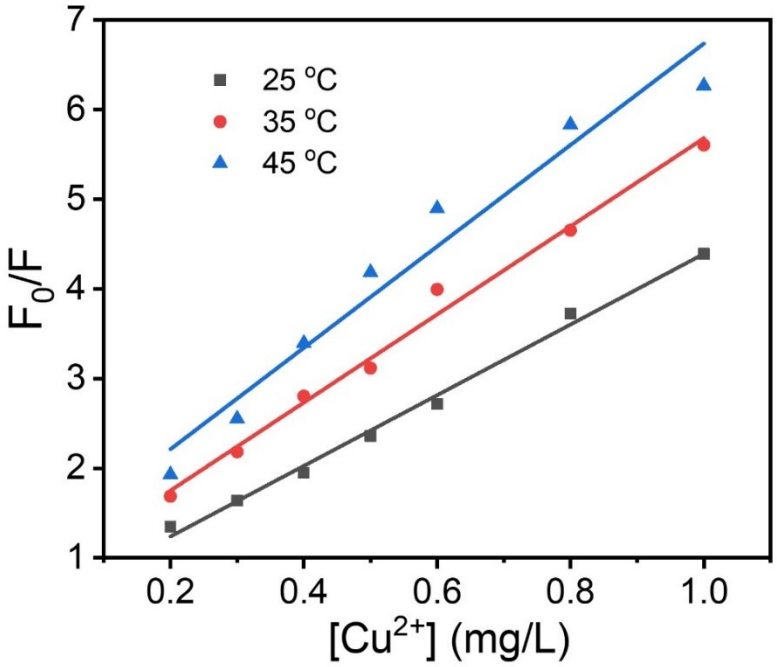

Fig. S6 Stern–Volmer plots for the fluorescence-intensity quenching by Cu^{2+} with MS-NSP at three different temperatures (25 °C, 35 °C and 45 °C).

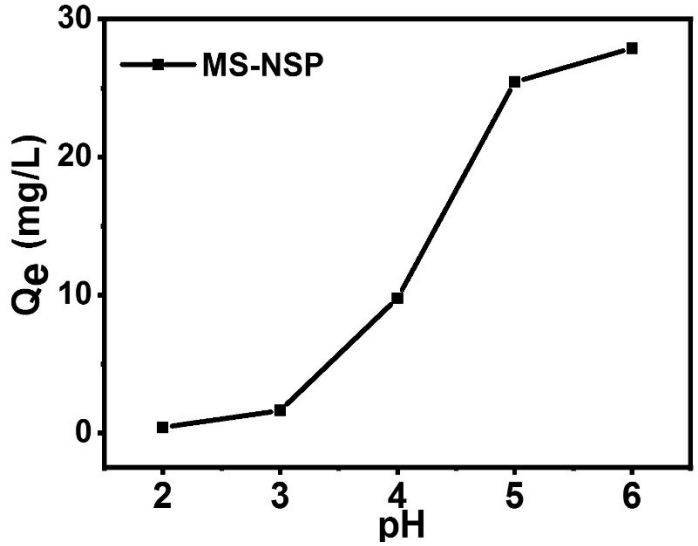

Fig. S7 Effect of pH on the adsorption capacity of MS-NSP for Cu^{2+} at 25 °C (MS-NSP: 1 mg/mL; initial Cu^{2+} concentration: 100 mg/L; 24 h).

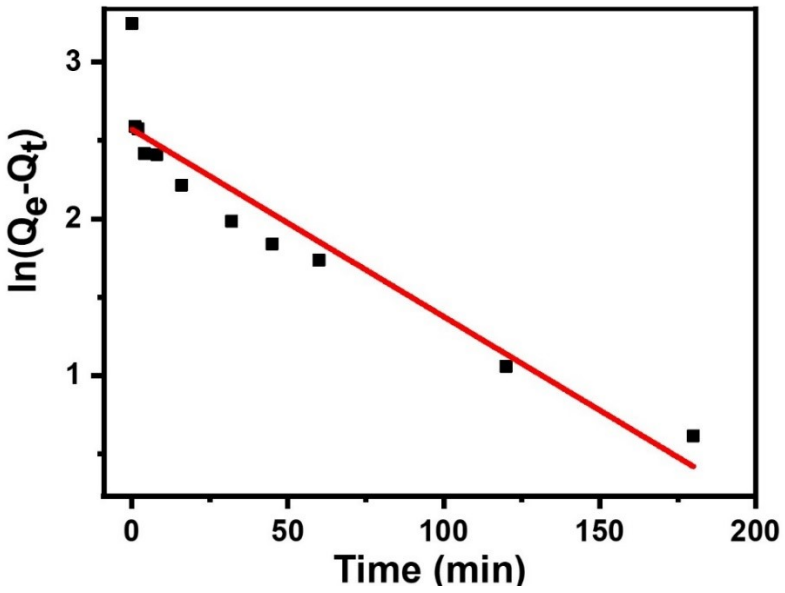

Fig. S8 Pseudo-first order kinetic curves for Cu^{2+} adoption on MS-NSP.

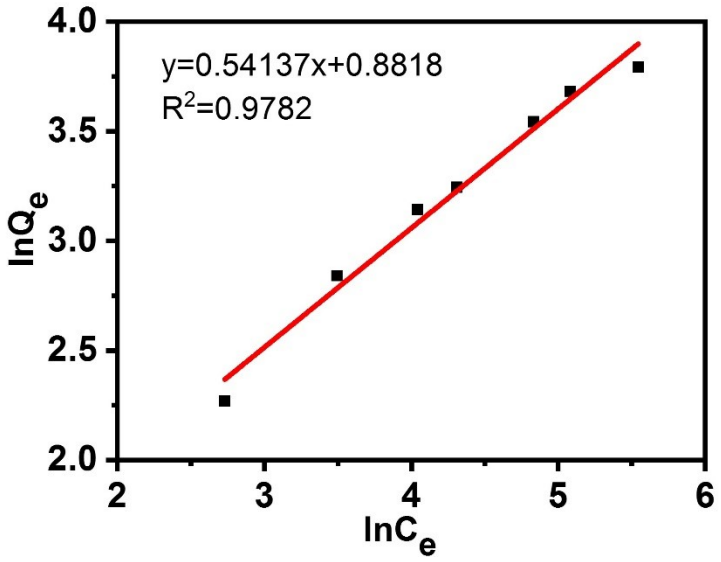

Fig. S9 Freundlish model plots for the adsorption of Cu^{2+} onto MS-NSP.

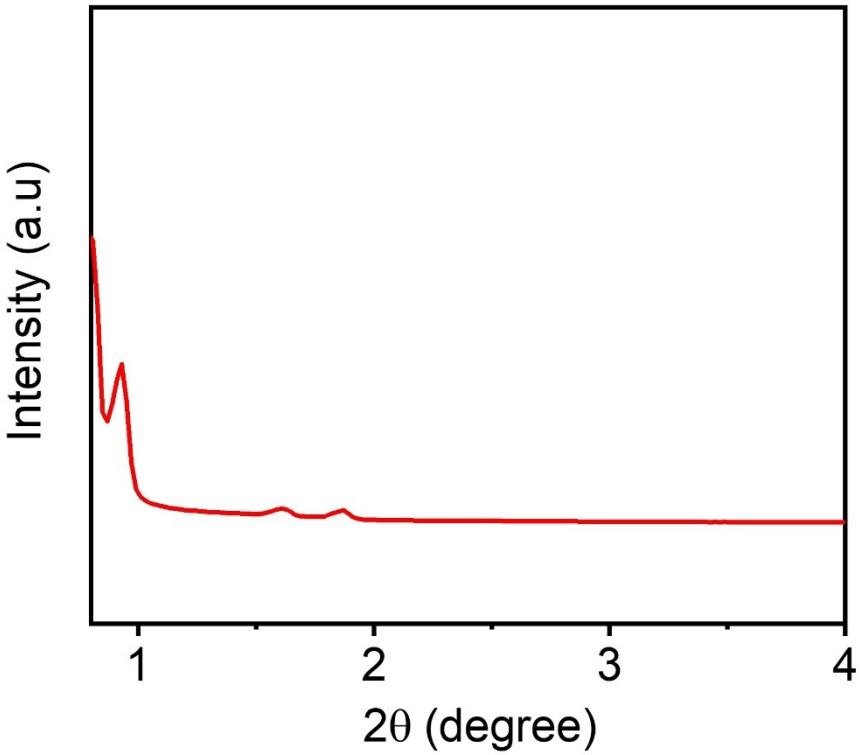

Fig. S10 Low-angle XRD patterns of regenerated MS-NSP after adsorption of Cu^{2+}.

References

[1] D. Herebian, K.E. Wieghardt, F. Neese. Analysis and Interpretation of Metal-Radical Coupling

in a Series of Square Planar Nickel Complexes: Correlated Ab Initio and Density Functional Investigation of [Ni(LISQ)2] (LISQ=3,5-di-tert-butyl-o-diiminobenzosemiquinonate(1-)), J. Am. Chem. Soc. 125 (2003) 10997-11005.
[2] Y. Zhou, L. Luan, B. Tang, Y. Niu, R. Qu, Y. Liu, W. Xu. Fabrication of Schiff base decorated PAMAM dendrimer/magnetic Fe3O4 for selective removal of aqueous Hg(II), Chem. Eng. J. 398 (2020) 125651.
[3] Q. Meng, X. Zhang, C. He, G. He, P. Zhou, C. Duan. Multifunctional Mesoporous Silica Material Used for Detection and Adsorption of Cu2+ in Aqueous Solution and Biological Applications in vitro and in vivo, Adv. Func. Mater. 20 (2010) 1903-1909.
[4] J. Isaad, A. El Achari. BODIPY modified silica coated magnetite nanoparticles as fluorescent hybrid material for Cu (II) detection in aqueous medium, Dyes Pigm. 99 (2013) 878-886.
[5] L.-L. Li, H. Sun, C.-J. Fang, J. Xu, J.-Y. Jin, C.-H. Yan. Optical sensors based on functionalized mesoporous silica SBA-15 for the detection of multianalytes (H+ and Cu2+) in water, J. Mater. Chem. 17 (2007) 4492-4498.
[6] D. Lu, J. Lei, Z. Tian, L. Wang, J. Zhang. Cu2+ fluorescent sensor based on mesoporous silica nanosphere, Dyes and Pigments 94 (2012) 239-246.
[7] X. Chen, A. Yamaguchi, M. Namekawa, T. Kamijo, N. Teramae, A. Tong. Functionalization of mesoporous silica membrane with a Schiff base fluorophore for Cu(II) ion sensing, Analytica Chimica Acta 696 (2011) 94-100.
[8] H. Jiang, Y. Liu, W. Luo, Y. Wang, X. Tang, W. Dou, Y. Cui, W. Liu. A resumable two-photon fluorescent probe for Cu2+ and S2− based on magnetic silica core-shell Fe3O4@SiO2 nanoparticles and its application in bioimaging, Anal. Chim. Acta 1014 (2018) 91-99.